Eindhoven University of Technology

BACHELOR

Plasmon-enhanced single-molecule fluorescence under saturated excitation intensity

Dedding, Lex M.

Award date:
2019

Link to publication

Disclaimer
This document contains a student thesis (bachelor's or master's), as authored by a student at Eindhoven University of Technology. Student theses are made available in the TU/e repository upon obtaining the required degree. The grade received is not published on the document as presented in the repository. The required complexity or quality of research of student theses may vary by program, and the required minimum study period may vary in duration.

General rights
Copyright and moral rights for the publications made accessible in the public portal are retained by the authors and/or other copyright owners and it is a condition of accessing publications that users recognise and abide by the legal requirements associated with these rights.

- Users may download and print one copy of any publication from the public portal for the purpose of private study or research.
- You may not further distribute the material or use it for any profit-making activity or commercial gain

EINDHOVEN UNIVERSITY OF TECHNOLOGY

Department of Applied Physics
Molecular Biosensing for Medical Diagnostics Research Group

Plasmon-enhanced Single-Molecule Fluorescence under Saturated Excitation Intensity

Bachelor End Project

L.M. Dedding (0946167)

Supervisors:
dr. Peter Zijlstra
Yuyang Wang MSc.

Eindhoven, June 2019

Contents

Chapter 1

Introduction

Experimental biophysical investigations have been traditionally performed on an 'ensemble average' level of cells or molecules. In an ensemble level experiment, it is usually assumed that the individual cells or molecules are identical physically and chemically. And by doing this, one uses a single metric for a population of biological samples, and any 'noise' that is caused by 'outliers' is smoothed out. However, There is a distinct downside to this method, since there may be valuable information hidden in the 'noise'. Ensemble averaging runs the risk of losing data on heterogeneity that is crucial for the understanding of the cellular/molecular interactions [14]. Analysing single molecules individually allows a better study of the underlying effects of some processes.

There are multiple ways of studying single molecules like atomic force microscopy or electron microscopy, but one of the least invasive techniques is single-molecule fluorescence microscopy (SMFM) [19]. SMFM has been widely used to study interactions and nanostructures in biology and material science. It is possible to measure processes in live cells [5]. SMFM can also be used to break the diffraction limit. For example, state-of-the-art super-resolution microscopy relies on the sequential blinking of single fluorescent molecules to localize features that are below the diffraction limit. Förster resonance energy transfer (FRET) for example, is a super-resolution microscopy technique based on the distance dependant energy transfer of multiple fluorescent molecules. FRET has been used to monitor lipid exchange on cell surfaces[11].

The high performance of SMFM relies on high quality single fluorescence molecules that ideally serve as bright and stable photon sources. However, almost in all experiments the brightness of the fluorophore is limited, which is due to the intrinsic photophysics of single molecules allowing a maximum number of emitted photons. The result is that the temporal resolution of typical single-molecule studies is limited to >10 ms. In this time range, it is possible to study process which typical have millisecond dynamics, including biomolecular interactions and slow conformational changes of proteins/DNAs [13]. However, it is extremely difficult to study process that have microsecond or less dynamics, for example fast conformational changes and single enzyme kinetics. The very limited amount of photons emitted in such very short time strongly restrict the accessible time domain SMFM can reach. Figure 1.1 schows the steps of protein folding and the respective timescales of these steps. The steps that take a shorter time than 10ms can not be monitored with unenhanced SMFM.

Therefore approaches to enhance the fluorophore brightness are urgently needed to enable investigations into fast dynamics. To study the amount of photons emitted by a single molecule, the fluorescence of individual single molecules must be characterized. Typically one can use fluorescence correlation microscopy (FCS) to study the fluctuation of single fluorescence molecules diffusing in and out of a laser focus. As a widely used alternative, wide-field fluorescence microscopy based on total-internal reflection fluorescence microscopy (TIRFM) can give excellent signal-to-noise ratio to allow enough contrast to visualize single fluorophores. It has been found that by combining an enzymatic oxygen-scavenger system and a redox pair, one can enhance the brightness by a factor between 1.4 and 24 depending on the PH [4].

Coupling the excitation and emission of single fluorescent molecules to plasmonic nanoparticles

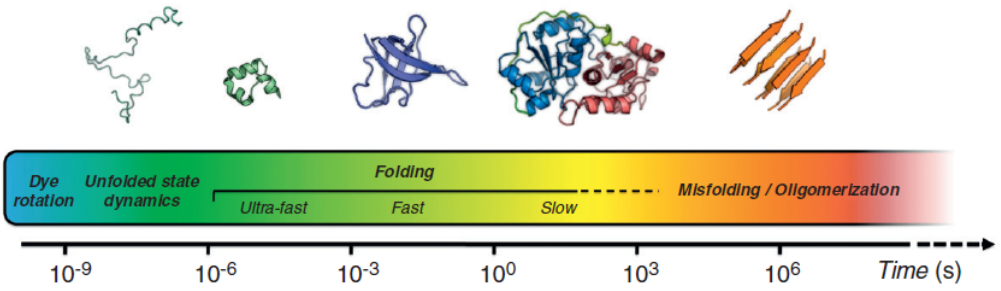

Figure 1.1: The timescales of the different steps in protein folding [13].

can also be used modulate the brightness, with the help of a process commonly known as plasmon-enhanced fluorescence (PEF). PEF strongly depends on the optical properties of single nanoparticles, and the photophysics of single molecules. For example, a fluorescence brightness enhancement of 1100 fold with a gold nanorod by matching the surface plasmon resonance of the nanorod with the excitation and emission wavelength of the fluorophore with low intrinsic quantum yield [17]. The advantages of enhancement of single fluorophores by coupling with plasmonic particles is that it is very versitile and relatively easy to implement. Plasmonic nanoparticles are suitable to study PEF since they is size- and shape-dispersion in a single drop of colloidal suspension, allowing one to study the complex wavelength dependencies of PEF, which will be discussed in chapter 2.

Chapter 2

Theoretical Background

2.1 Photophysics of single molecules

Fluorophores are fluorescent molecules capable of emitting light after excitation. The complex photophysics asscociated with the emission and excitation can be simplified by a two-level energy scheme. First, a photon is absorbed by the molecule causing the molecule to go from the ground state S_0 to a higher excited vibrational state S_1'. Then the molecule relaxes from S_1' to a lower vibrational state S_1 by internal conversions and vibrations without emitting a photon. That energy is lost to the solvent molecules around the fluorophore. In the last step, the excited state S_1 relaxes to the ground state by either emitting a photon or by transferring its energy another way [7]. The steps are schematically represented in Figure 2.1.The fraction of relaxation by emitting a photon compared to the total relaxations is called the quantum yield and is given by the following formula [15]:

$$\phi = \frac{\gamma_r}{\gamma_r + \gamma_{nr}}, \tag{2.1}$$

with γ_r the radiative decay rate $[s^{-1}]$ and γ_{nr} the non-radiative decay rate $[s^{-1}]$. Because S_1 has a slightly lower energy than the S_1' that the ground state was excited to, the energy of the emitted photon is slightly lower than the photon that was used to excite the fluorophore. This lower energy translates into a longer wavelength. Absorption and emission spectra clearly show this shift in wavelength such as in Figure 2.2. This wavelenght shift is called the Stoke's shift [10]. The figure shows a distribution of absorption and emission wavelength in contrast to the discrete wavelengths expected from the simplied model described above.

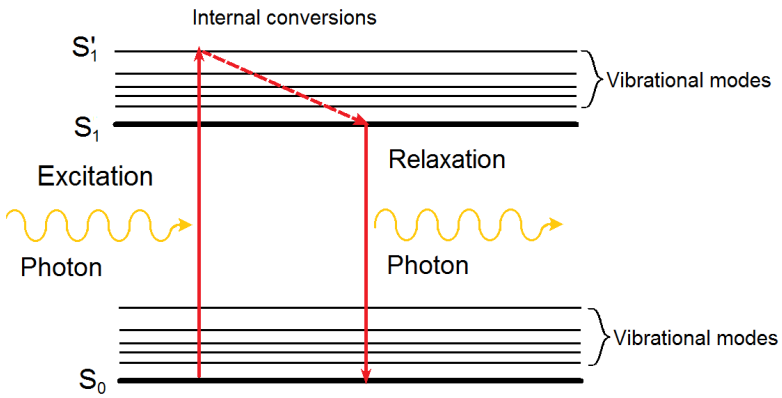

Figure 2.1: A schematic representation of the process of fluorescence. Note that it is also possible for a relaxation without the emission of a photon.

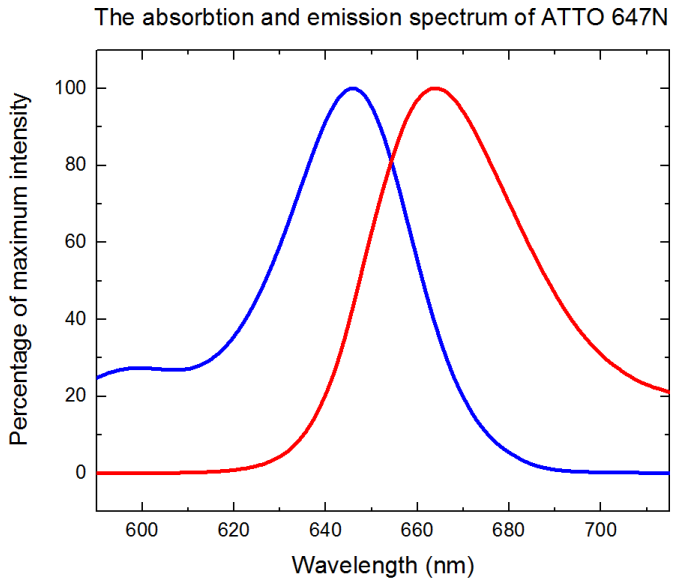

Figure 2.2: The absorbtion (Blue line) and emission (Red line)spectra of ATTO 647N, the fluorophore used in this experiment, according to the manufacturer [1]

The time a fluorophore is in its excited state before relaxing is called the fluorescence lifetime. The florescence lifetime is given by: $\tau = (\gamma_r + \gamma_{nr})^{-1}$ [9]. The shorter the lifetime, the more times the fluorophore can excite and relax again in a second, provided the dye is excited with sifficient photons per second. Under very high excitation rates, saturation occurs because then the fluorophore is still in an excited state when the next photon arrives and can not be excited by that photon..

The amount of measured photons in an experimental setup, or photon count rate (PCR), is given by the following formula at low excitation intensities [15][16]:

$$PCR = \eta \frac{\sigma}{h\nu} \phi I_E, \tag{2.2}$$

with η the collection efficiency of the optical system, σ the the absorption cross section of the fluorophore $[m^2]$, $h\nu$ the energy of the photon $[J]$, and I_E the excitation intensity $[Wm^{-2}]$. Here the PCR increases linearly with the excitation intensity. If the excitation intensity increases and saturation occurs, equation 2.2 changes to equation 2.3:

$$PCR = \eta \frac{\sigma}{h\nu} \phi \frac{I_E I_{sat}}{I_E + I_{sat}}, \tag{2.3}$$

with I_{sat} the saturation intensity of the fluorophore in W m^{-2}. Equation 2.3 is plotted in figure 2.3 to show the effect of different saturation intensities. The saturation intensity can be calculated by[15]:

$$I_{sat} = \frac{(\gamma_r + \gamma_{nr})h\nu}{2\sigma}. \tag{2.4}$$

If the illumination intensity of a fluorophore is very high, the fluorophore can go to a different state that is not depicted in figure 2.1. It can stay in that state for a very long time, while not emitting a photon, compared to the S_1 state. A fluorophore in that state is called bleached.

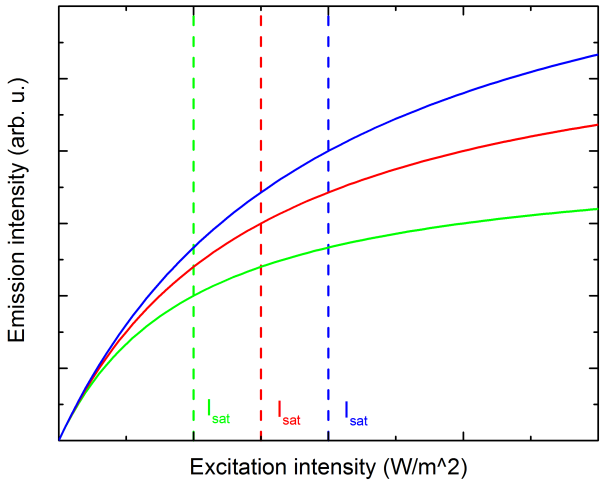

Figure 2.3: Equation 2.3 plotted for three different arbitrary fluorophores and their saturation intensity depicted as a dashed line with its color corresponding to the fluorophore. Notice that if the saturation intensity increases, the emission intensity decreases slower for high excitation intensities.

2.2 Surface plasmon resonance

Electromagnetic waves such as light can interact with the free conduction electrons of a metal particle causing the electrons to oscillate. If the wavelength of the electromagnetic wave is a lot longer than the particle itself, the entire cloud of free electrons in the material oscillates in phase.[6] [19]. Since the mass of the particle is a lot larger than the mass of the electrons, the particle stays stationary while the electron cloud oscillates.

The negatively charged electrons are pulled away from the positively charged atoms which creates a restoring force much like a spring [19]. This restoring force is dependant on the shape, the material of the particle and on the dielectric surrounding the particle. If those properties match with the wavelength incident electromagnetic wave, resonance can occur. This is called Surface Plasmon Resonance (SPR). The particle scatters light most strongly at the SPR wavelength.

For silver, copper and gold nanoparticles, SPR is possible with visible light making them usable in optical applications[6]. However, since copper and silver are prone to oxidation, and therefore change the shape and surface properties, gold is usually more suitable for practical applications such as the experiments in this report. Also, modern fabrication techniques make it possible to finely tune the size and aspect ratio of nanoparticles, making it possible to fabricate particles with the SPR wavelength that is required for an experiment [19]. There is still some heterogeneity in an ensemble of fabricated nanoparticles as can be seen in figure 2.4. A consequence of this heterogeneity is that the SPR wavelengths of an ensemble of nanorods will be heterogeneous as well.

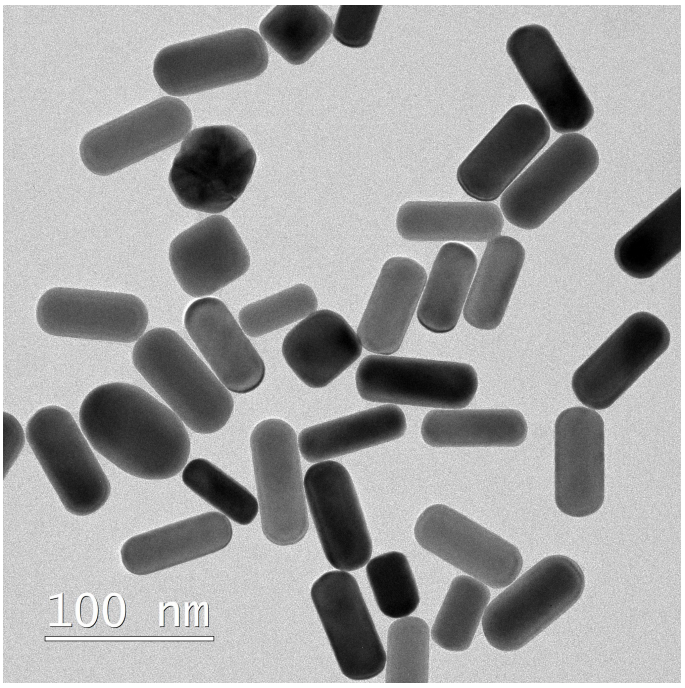

Figure 2.4: A transmission electron microscopy image of an ensemble of gold nanorods.

2.3 Plasmon enhanced fluorescence

The SPR enhances the electromagnetic field around the nanorod when it is irradiated by the a light source with a similar wavelength as the SPR wavelength of the particle. This enhancement of the electromagnetic field is location-dependent and is largest around the tips of the nanorod. Multiple numerical simulations show this with varying enhancements depending on the size of the nanorod and the incident wavelength [8][17][18].

This electromagnetic field enhancement has multiple effects on the fluorescence of fluorophores near the surface of a nanorod. One of the effects is an increase in the excitation of the fluorophores causing an increase in fluorescence. Figure 2.5 (a) and (b) are examples of a numerical simulation of the excitation enhancement [15]. Also, both the radiative and non-radiative decay rates are increased close to the tip of the nanorod [8]. Higher decay rates increase the saturation intensity (2.4) and thus increase the PCR of the fluorophore(2.3). The excitation enhancement is greatest when the SPR of the nanoparticle has the same wavelength as the excitation wavelength of the particle. The decay rate enhancement is greatest when the SPR matches the relaxation wavelength of the fluorophore.

Close to the surface of nanoparticles the quantum yield of fluorescent dyes is decreased significantly because nonradiative decay increases. This effect can completely quench fluorescence on the surface of nanoparticles but quickly decreases with an increased distance [3]. Further away from the surface, the quantum yield can actually be enhanced by the effects of the nanorod. This effect is greater for phluorophores that start with a relatively low quantum yield since the theoretical maximum quantum yield can never be more than 1. The emission enhancement and quenching is displayed in Figure 2.5 (c) and (d) for two different fluorophores with a different starting quantum yield.

These effects combined cause a location dependant fluorescnence enhancement close to the tips of the nanorod. As displayed in Figure 2.5 (e) and (f). The maximal possible fluorescence enhancement possible is a trade-off between the increased fluorescence close to the tips of the nanorod and the quenching effect close to the surface. Furthermore, at low excitation intensities far below saturation, the enhancement is greatest when the SPR matches the incident wavelength because

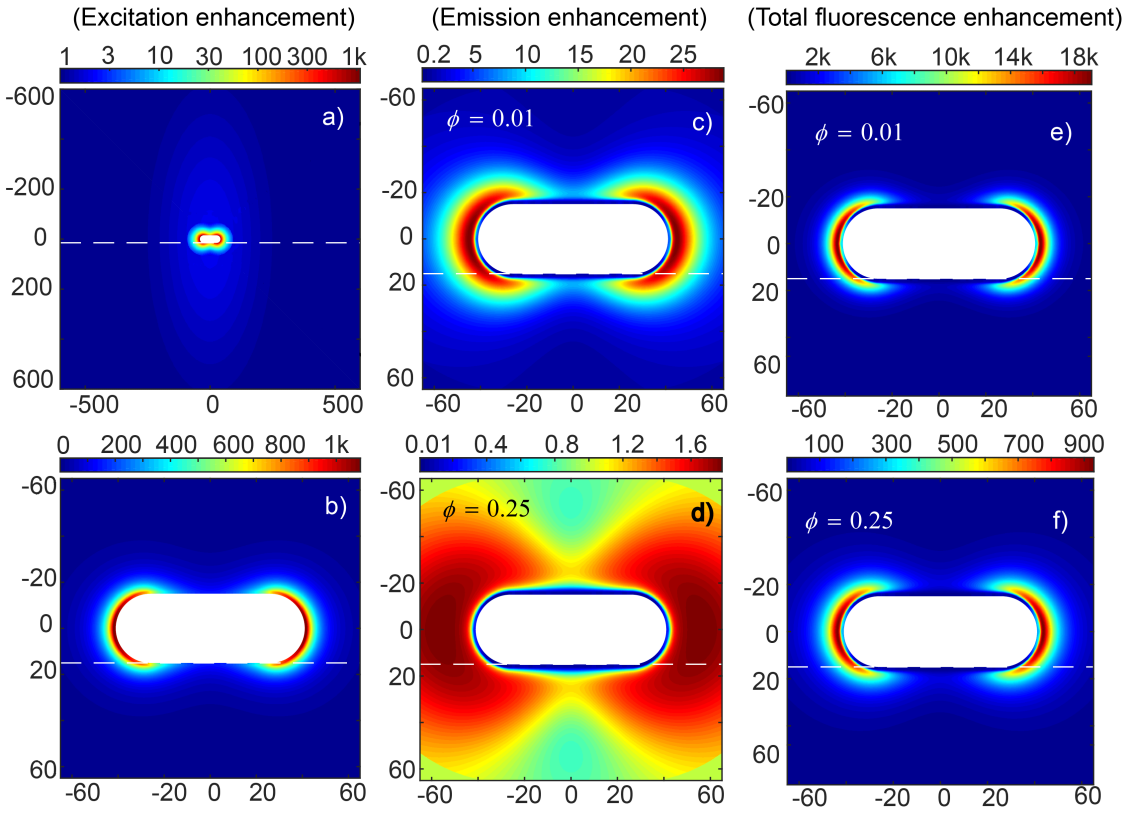

Figure 2.5: (a) and (b) show the location dependant excitation enhancement of a 82 × 30 nm^2 gold nanorod compared to the incident intensity of a 705 nm wave. The SPR of the goldnanorod is 705 nm. (c) and (d) show location depentand the quantum yield enhancement of two fluorescent emitters with a starting quantum yield of 0.01 and 0.25 respectively. (e) and (f) shows the combination of the effects on the total fluorescence enhancement for the same nanorod and emitters.[15]

then the excitation intensity is increased. At excitation intensities above saturation however, this effect is less noticeable and the fluorescence enhancement benefits most from a SPR matching the relaxation wavelength causing a shorter lifetime. In figure 2.6 this SPR dependant enhancement is plotted.

The photon count rate enhancement was theoretically evaluated based on the PCR calculation of unenhanced and enhanced single fluorophore bound to 3 nm away from the tip of gold nanorods with aspect ratio of 2.3, and fixed width of 30 nm. For unenhanced photon count rate, the calculation was done according to equation 2.3 with an illumination intensity of 100 time saturation intensity, where the overall collection efficiency was $\eta = 8\%$, absorption cross section $\sigma = 1 \times 10^{-20}$ m^2, quantum yield $\phi = 0.5$. For enhanced photon count rate, a numerical simulation of the fluorescence enhancement was performed using a boundary element method using the MNPBEM toolbox for Matlab. Single nanoparticles with different geometries were embedded in a non-absorbing dielectric medium with the defractive index of water (1.33). The dielectric function of gold was interpolated from the Johnson-Christy database. The modified near field and decay rates were calculated with an 637nm excitation and 670 nm emission of the molecule, approximated as an electric dipole.

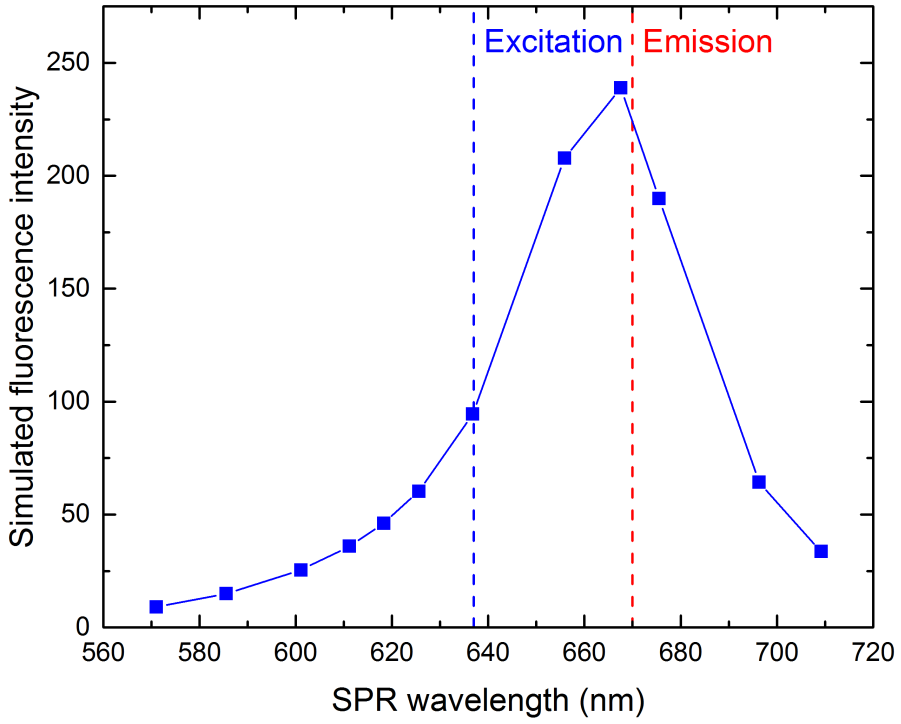

Figure 2.6: The simulated fluorescence enhancement is plotted for different SPR wavelengths of the nanorods at an excitation intensity of 100 times the saturation intensity.

Chapter 3

Method and Setup

3.1 TIRF Microscopy

For the experiments, a total internal reflection fluorescence (TIRF) microscopy was used. TIRF is ideal to perform single molecule measurements due to low fluorescence background [12]. TIRF microscopy relies on the creation of an evanescent field on the interface between two media with different refractive indexes. In this case glass ($n_g \approx 1.51$) and water ($n_w \approx 1.33$) [12]. When a light source hits an interface with an angle larger than the critical angle, light is totally internally reflected. By solving Maxwell's equations, it can be found that the electromagnetic field slightly penetrates the medium and creates a so-called evanescent field. This field decays drastically away from the surface, and typical penetration depth of a a few 100 nm. This very thin sheet of light is then used to excite the SPR of the nanorods and fluorescence only when fluorophores are close to the surface. This property is what makes TIRF suitable for single molecule microscopy.

In the case of these experiments, the angle of incidence on the plane should be at least 61.7°as can be determined by Snell's law [2]. A right isosceles prism is used to minimize any reflection before the total internal reflection on the interface. After considering this triangle, the maximum angle the incident light can have compared to the slide, is 19.2°. At this angle, the penetration depth is the greatest.

The relative intensity of the evenescant field decays exponentially by the following formula [12]:

$$I = I_0 e^{-z/d}, \tag{3.1}$$

with I_0 (W m^{-2})the incoming intensity of the incident light. z (m) the distance away from the plane of incidence and d (m) the penetration depth of the evanescent field in the media given by:

$$d = \frac{\lambda_0}{4\pi\sqrt{n_g^2 sin^2\theta_i - n_w^2}}, \tag{3.2}$$

with λ_0 (m) the wavelength of the incoming light in vacuum and θ_i (°) the angle of incidence. In the following calculations, of an angle 1% larger than the perfect TIRF angle was considered. In these experiments with a laser wavelength of 637nm, the penetration depth d will be 355 nm. Since the nanorods are 30nm in width and the maximum intensity of the electric field enhancement is in the middle of the tips of the nanorods, the relative intensity of the to be enhanced field is approximated to 0.96 times the evanescent field intensity. This is a negligible difference and will not be taken into account.

The intensity of the evanascent field is polarisation dependant, but since the laser illuminiting the sample has a parallel polarization, only that intensity will be taken into account. The parallel intensity of the evanascent field is given by:

$$I_0^{\parallel} = I_i^{\parallel} \frac{4cos^2\theta_i(2sin^2\theta_i - (n_w/n_g)^2)}{(n_w/n_g)^4 cos^2\theta_i + sin^2\theta_i - (n_w/n_g)^2}, \tag{3.3}$$

with $I_i^{\parallel}$ the intensity of the incoming light source in W m^{-2}. In the case of these experiments, the evanescent wave intensity will be about 4.9 times times larger than the illuminating light intensity.

For the experiments, an electron−multiplying (EM) gain of 50 was used combines with an integration time of 100ms. Photon conversion was performed with the help of the photon counting mode of Andor Solis software. Two images were taken to acquire the conversion factor. An image under the photon counting mode was taken, and compared to the image taken under normal EM gain mode in Nikon NIS element software. A conversion factor of 3.51 was found.

3.2 Samples

The gold nanorods are spincoated on thiolated glass and fixated there. Then the particles are covered with single-stranded DNA moelcules with 30 nucleotides (termed docking strands). The sample is placed in a flow cell that is placed underneath the prism used for TIRF imaging. A solution of single-stranded DNA labeled with a ATTO 647N at the $5^{'}$ end (termed imaging strands) is flushed through the flow cell. The imaging strands have 9 nucleotides that are complementary to the docking strands. A nanorod, covered in docking strands, has been schematically displayed in figure 3.1. The fluorophore-labeled imaging strands will randomly bind to docking strands on the nanoparticles between 3 and 5 nm away from the surface. This way some will bind on the most ideal enhancement location. A more detailed description of the slide preparation can be found in appendixA.1.

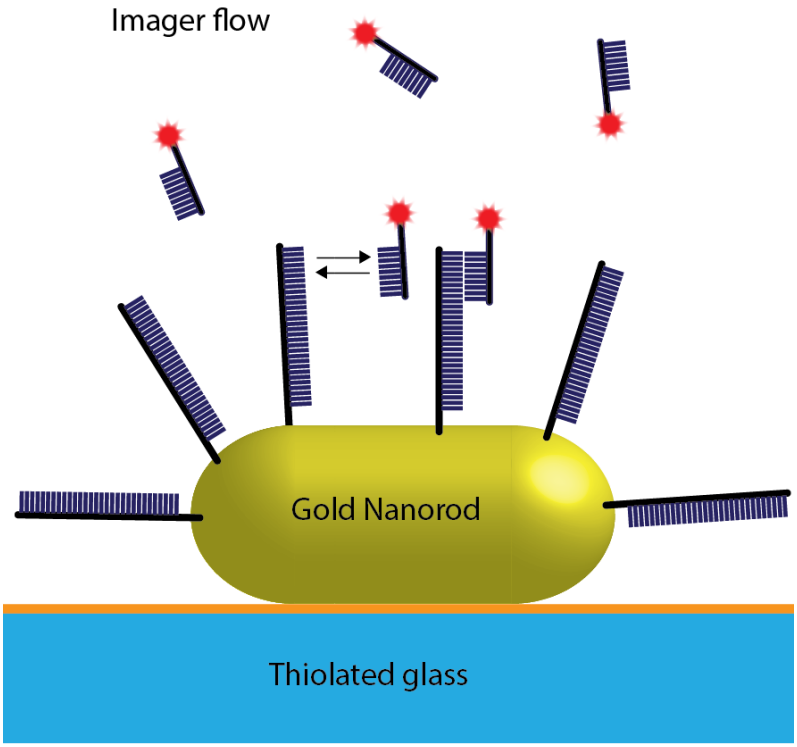

Figure 3.1: A schematic representation of a fixated gold nanorod covered in docking strands. Note that the DNA strands are not the same scale as the nanorod.

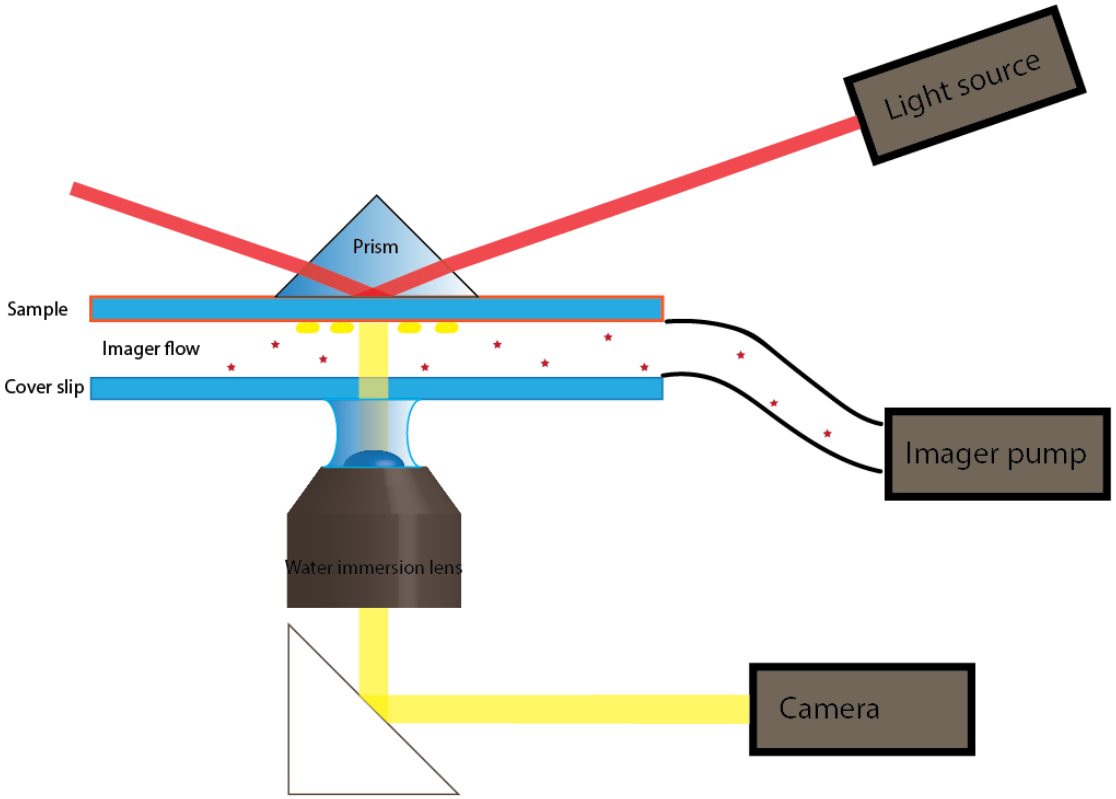

Figure 3.2: A schematic of the setup used in the experiments. Note the light source can be either a white light source or a laser.

3.3 Single nanoparticle spectroscopy

The coverslip immobilized gold nanorods is illuminated with white light, as shown in figure 3.2, and a series of images is taken with different bandpass filters of different wavelengths. By doing this, the intensity of different wavelengths for all particles in the field of view can be determined. The SPR of the particles can then be determined by analysing these intensities. Afterwards, single nanorods are selected for further analysis based on their Lorentzian lineshapes.

3.4 Unenhanced single molecule fluorescence

To determine the factor of fluorescence enhancement, the brightness of unenhanced molecules must be established. This is done by measuring the fluorescence intensities of single imager strand without the presence of gold nanorods. The imagers are flushed through the flow cell in the same rate as the nanorod samples and under a mean excitation intensity from $1.1 \times 10^5 W/m^2$ to $6.4 \times 10^6 W/m^2$. Imagers strands randomly stick to the glass surface, and appear as diffraction-limited spots in the EMCCD camera. A video for different laser intensities is taken and approximately 10^5 sticking imagers per illumination intensity are localized and fitted with a 2D Gaussian function. The volumes under the 2D Gaussian are then calculated to be the fluorescence intensities. The different laser intensities are location dependant because the illuminating laser has a Gaussian intensity profile. The corresponding illumination intensity was calculated by fitting the background with the following Gaussian 2d function:

$$Background = B + Me^{-\frac{(x-x_0)^2}{2\sigma_x^2} - \frac{(y-y_0)}{2\sigma_y}}, \tag{3.4}$$

with B a base level, M the maximum illumination intensity, x and y the coordinates of the image, x_0 and y_0 their respective offsets and σ_x^2 and σ_y^2 the respective variances. This fitted function is then normalized with the total illumination intensity of the laser to make the function in W/pixel and divided by the pixel surface to get W/m^2. This intensity is then multiplied with a factor of 4.9 because the evanescent field close to the other side of the surface is 4.9 times larger than the illuminating field [12].

3.5 Fluorescence enhancement measurement

After determining what particles in the field of view are single particles and what their SPR wavelength is, the sample is illuminated with a 637nm laser instead of the white light. A 650nm high pass filter is installed to filter out the laser light but still let the emmission wavelength of the fluorophores through. A video is taken to get a photon count rate timetrace for every particle. When a fluorophore binds to the particle, a photon count rate peak is expected because of the light emitted by the fluorophore. The highest peaks are expected when a fluorophore binds to the tips of the nanorod. This is however impossible to direct because both the docking strand binding and the coupling of the fluorophore is completely random.

Chapter 4

Results and Discussion

4.1 Gold nanorod SPR wavelength

Figure 4.1 shows the measured spectrum of one of the particles and the corresponding fit. This was done for all particles recognised by the script and particles which showed a proper fit were then labeled as "single particles" and processed further. One of the measured particles and its corresponding fit has been plotted in figure 4.1

The gold nanorods that are used for the experiment are about 60 × 30 nm^2. According to the manufacturer the mean SPR is 650 nm, but after measuring the spectra of an ensemble of 868 particles a mean SPR of 667 was found with a standard deviation of 22. The distribution can be found in figure 4.2. The reason for this shift can be attributed to the attachments of the particles to the glass. Glass has different dielectric properties than water which change the SPR wavelength.

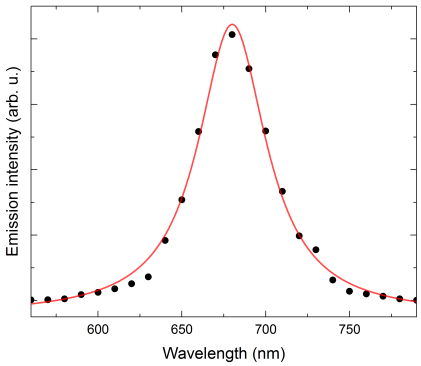

Figure 4.1: A graph showing the scattering spectrum of a gold nanorod with an SPR wavelength of 680nm

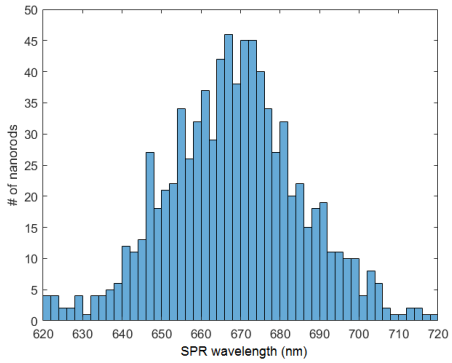

Figure 4.2: The histogram shows a peak of SPR wavelength around 670nm instead of the 650nm according to the manufacturer.

4.2 Unenhanced single fluorophore photon count rate

The illumination intensity was determined by the fit discussed in section 3.4. But because the fit of the illumination intensity deviated too much from the real value to accurately calculate the location dependant illumination intensity, the mean value illumination intensity was used to plot figure 4.3. The mean illumination intensity is the full width half maximum value of the fitted

function. Despite the large standard deviation in the photon count rate, caused by a range of illumination intensities, the results clearly show a saturation effect according to equation 2.3. The saturation intensity is about 6.7×10^6 W m^{-2} with an uncertainty of 0.5×10^6.

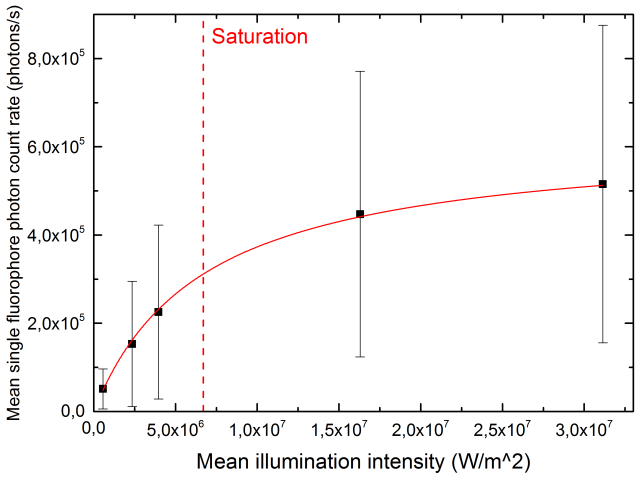

Figure 4.3: The mean single fluorophore photon count rate for the mean illumination intensity and the fit of equation (2.3). The dashed line shows the saturation intensity at 6.7×10^6 W m^{-2}.

4.3 SPR dependency

Of the video that was taken of the gold nanorod sample illuminated with the laser, a region of interest (ROI) was selected to ensure the illumination intensity was more homogeneous. In this ROI 55 single particles resided with an illumination intensity deviating no more than 10 percent from the median. The median illumination intensity in the ROI was approximately 6×10^7W m^{-2} so about 8 times saturation intensity. Of these particles, the photon count rate was calculated for every frame of the video. This so called "timetrace" of three particles with different SPR wavelengths have been plotted in figure 4.4. As can be seen, the timetraces have a steady noise level and intensity peaks. These peaks occur when a fluorophore binds to the nanorod and is enhanced. Because the fluorophores bind to random locations on the nanorod, at random distances and for random times, not every peak has the same size. Also, a clear difference in the mean burst photon count rates can be observed for the different particles.

To calculate the photon count rate of a fluorophore binding to the nanorod, the top of the intensity peaks were subtracted by the base noise level. This value will be referred to as a burst from now on. The top 10 bursts were selected and those average values were plotted vs the SPR wavelenght of the corresponding particles in figure 4.5. The simulated fluorescence enhancement shown in figure 2.6 is also plotted in the same graph. The measured results clearly follow the simulated pattern although the emission peak is "red-shifted" about 10 nm.

The enhancement of the fluorophores by the single particles is about 2 to 14. This is a lot less than the calculated theoretical result. As discussed before, one of the reasons these particles might deviate from the theoretical simulations is that the fluorophores bind at random locations on the particle. The fluorescence enhancement is largest at the tips of the particles. If for some reason the fluorophores bind to a less favourable location, the enhancement will be less. Also, the mean value of the maximum bursts is taken which will be smaller than the maximum value. It is also possible that the burst is shorter than the integration time of the camera which will be discussed in more depth in section 4.4.

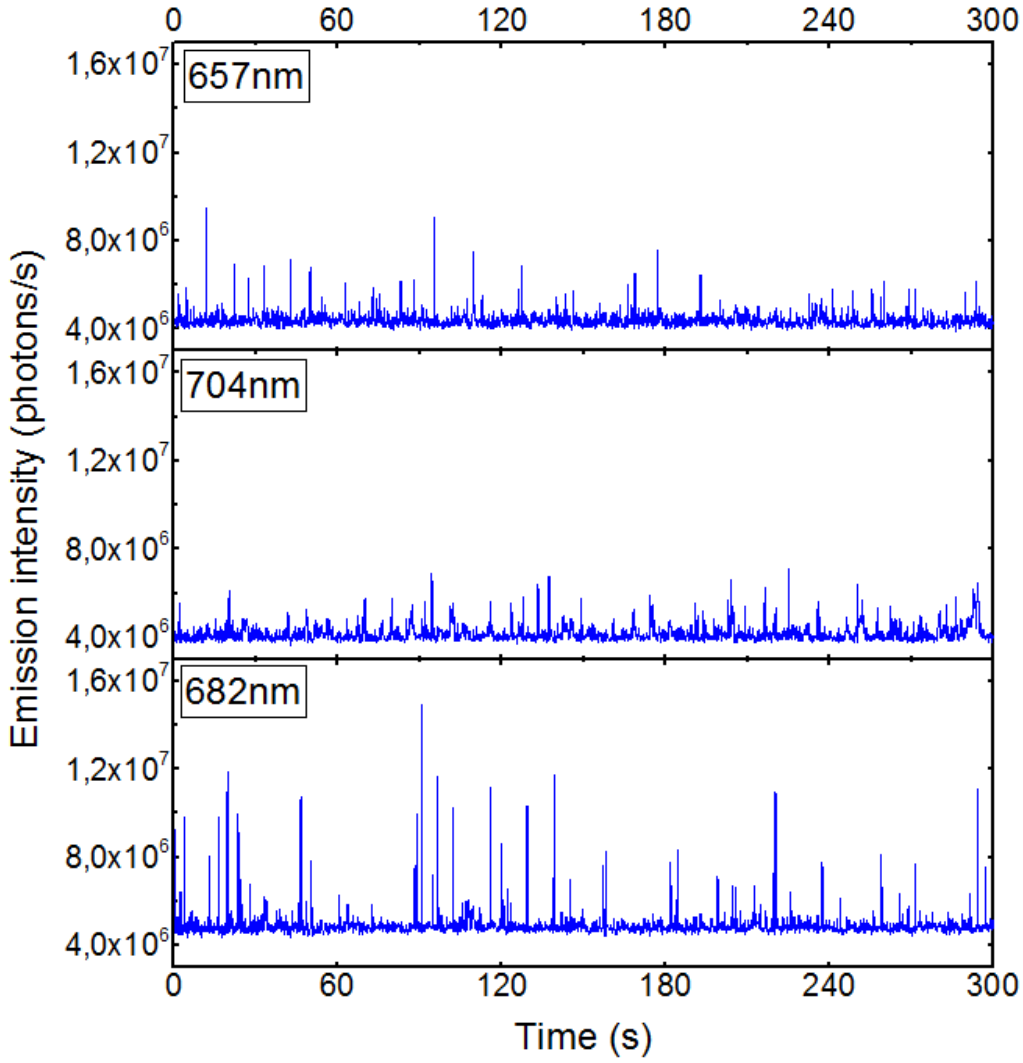

Figure 4.4: The timetraces of the intensity in the ROI around the particles for 3 different single particles with their corresponing SPR wavelengths. There is a clear difference in the height of the emission bursts.

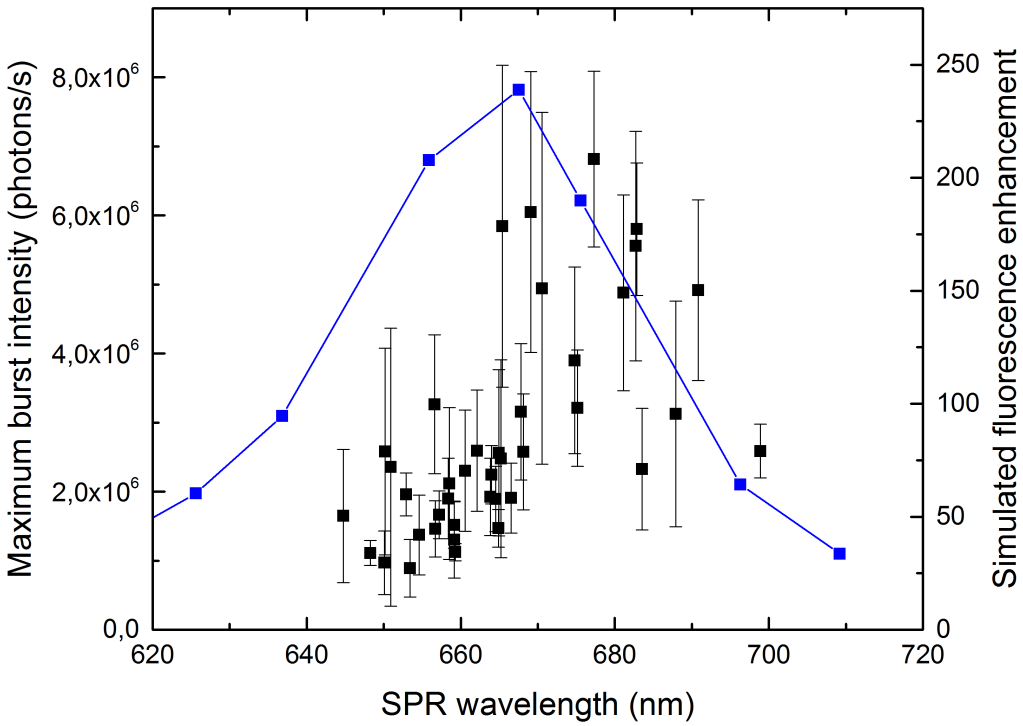

Figure 4.5: The max burst photon count rates for the single particles in the ROI illuminated by a 100mW laser. The simulated SPR wavelength dependant maximum fluorescence intensity enhancement is also plotted in the same graph in blue.

4.4 Integration time dependency

Upon closer inspection of the timetraces, it was noticed that a lot of bursts were only one frame long, especially at high illumination intensities. This could mean that bursts were shorter than the integration time of the camera. Either because the time the fluorophores are bound to the particle is too short or because the fluorophores are bleached too quickly. If either of those possibilities is the case, then the measured maximum intensity is smaller than the real value. The integration time is a trade off however. If the integration time is too short, the signal to noise ratio is expected to decrease. Also, at a smaller integration time the dead time of the camera is proportionally larger than for large integration times.

To explore this further, timetraces of another sample were measured with different integration times. In every measurement, the sample was illuminated by a 100mW laser corresponding to an average illumination intensity of approximately $6 \times 10^7 \mathrm{W\ m^{-2}}$. The signals were multiplied with a factor corresponding to the integration times to transform the signal into photons per second. The timetraces of one particle for two different integration times were plotted in figure 4.6. It is clear that the measurement performed with an integration time of 10ms has a lot more noise. This was expected since a larger integration time evens out noise more. Also there is a lot more heterogeneity in the burst photon count rate for the shorter integration time measurement.

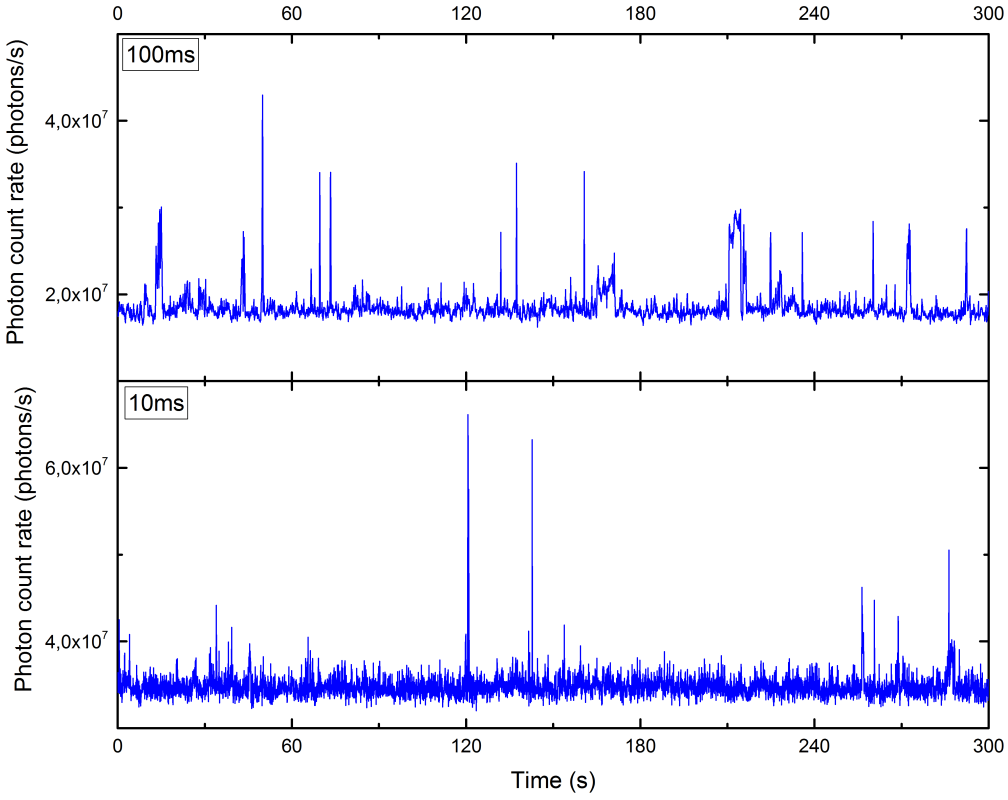

Figure 4.6: The timetraces of the same particle for different measurements, one with an integration time of 100ms and one with an integration time of 10ms.

The maximum burst photon count rates of the timetraces were calculated for the different

integration times with the same method as in section 4.3 and are plotted on a integration time log scale in figure 4.7. The graph shows a peak at an integration time of 40ms. However, the standard deviation in the maximum bursts has increased significantly as well. The maximum burst photon count rates were lowest for an integration time of 200ms as would be expected since there the burst was more evened out along with the noise. The larger error bars for the lower integration times can be caused by the heterogeneity in the burst photon count rates also seen in figure 4.6.

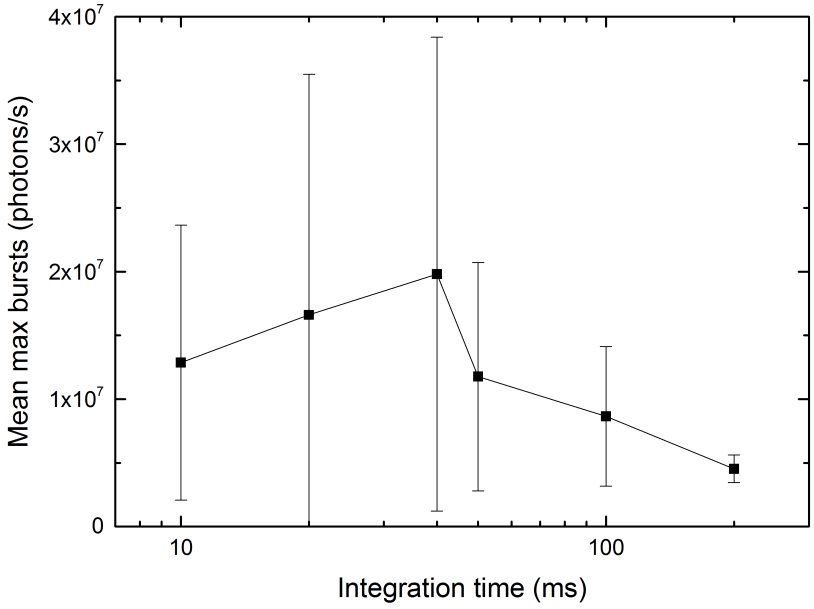

Figure 4.7: The mean maximum burst values for different integration times.

4.5 Sample decay

The above mentioned measurements were conducted in sequence. This was necessary to match the measured SPR wavelengths with the particles to determine whether they were single particles or not. This does mean that the sample was continuously illuminated for over an hour with a 100mW laser. This might have overheated the sample causing some docking strands to detach. This could explain why the 10ms integration time timetrace in figure 4.6 has about half the bursts as the 100ms integration time measurement as the 10ms integration time measurement was performed later.

Chapter 5

Conclusions

A pattern for SPR wavelength dependant fluorescence enhancement similar to theoretical simulations has been found. Above saturation illumination intensities the fluorescence enhancement of single fluorophores is greatest (14 times)for nanorods whose SPR wavelength is closest to the emission wavelength of the fluorophore. Even though the amount of enhancement wasn't a high as theoretically simulated due to uncontrollable factors, like how many fluorophores bound to the particles and on what locations. The pattern of the simulations was clearly in the measured results. Future measurements over longer times could increase the accuracy by providing more statistics.

Future measurements should be done with an integration time of 40 to 50 ms for more accurate results. These integration time give the highest maximum bursts intensities because the intensity of the short bursts isn't spread out over a longer time.

Enhancing the fluorescence of single fluorophores greatly increases the temporal resolution of single molecule fluorescence microscopy. This can have widespread applications in the measurement of many fast biophysical processes.

Bibliography

[1] ATTO-TEC. Fluorescence spectra atto647n, 2019. [Online; accessed April 26, 2019]. 4

[2] C.A. Bennett. *Principles of Physical Optics*. Wiley, 2008. 9

[3] Palash Bharadwaj, Pascal Anger, and Lukas Novotny. Nanoplasmonic enhancement of single-molecule fluorescence. *Nanotechnology*, 18(4):044017, 2006. 6

[4] Barbara H Davis, Linda M Link, and John E Hoots. Method of enhancing the fluorescent signal of a fluorescent oxygen scavenger, May 20 2003. US Patent 6,566,139. 1

[5] Bo Huang, Mark Bates, and Xiaowei Zhuang. Super-resolution fluorescence microscopy. *Annual review of biochemistry*, 78:993–1016, 2009. 1

[6] Prashant K Jain, Xiaohua Huang, Ivan H El-Sayed, and Mostafa A El-Sayed. Review of some interesting surface plasmon resonance-enhanced properties of noble metal nanoparticles and their applications to biosystems. *Plasmonics*, 2(3):107–118, 2007. 5

[7] Romdhane Karoui and Christophe Blecker. Fluorescence spectroscopy measurement for quality assessment of food systemsa review. *Food and Bioprocess technology*, 4(3):364–386, 2011. 3

[8] Saumyakanti Khatua, Pedro MR Paulo, Haifeng Yuan, Ankur Gupta, Peter Zijlstra, and Michel Orrit. Resonant plasmonic enhancement of single-molecule fluorescence by individual gold nanorods. *ACS nano*, 8(5):4440–4449, 2014. 6

[9] Joseph R Lakowicz, Yibing Shen, Sabato D'Auria, Joanna Malicka, Jiyu Fang, Zygmunt Gryczynski, and Ignacy Gryczynski. Radiative decay engineering: 2. effects of silver island films on fluorescence intensity, lifetimes, and resonance energy transfer. *Analytical biochemistry*, 301(2):261–277, 2002. 4

[10] Ming Li, Scott K Cushing, and Nianqiang Wu. Plasmon-enhanced optical sensors: a review. *Analyst*, 140(2):386–406, 2015. 3

[11] Luis Loura and Manuel Jose Prieto. Fret in membrane biophysics: An overview. *Frontiers in physiology*, 2:82, 2011. 1

[12] ML Martin-Fernandez, CJ Tynan, and SED Webb. A pocket guideto total internal reflection fluorescence. *Journal of microscopy*, 252(1):16–22, 2013. 9, 12

[13] Benjamin Schuler and Hagen Hofmann. Single-molecule spectroscopy of protein folding dynamicsexpanding scope and timescales. *Current opinion in structural biology*, 23(1):36–47, 2013. 1, 2

[14] Sviatlana Shashkova and Mark C Leake. Single-molecule fluorescence microscopy review: shedding new light on old problems. *Bioscience reports*, 37(4):BSR20170031, 2017. 1

[15] Yuyang Wang and Peter Zijlstra. Plasmon-enhanced single-molecule enzymology. *ACS photonics*, 5(8):3073–3081, 2018. 3, 4, 6, 7

[16] Emilie Wientjes, Jan Renger, Richard Cogdell, and Niek F van Hulst. Pushing the photon limit: nanoantennas increase maximal photon stream and total photon number. *The journal of physical chemistry letters*, 7(9):1604–1609, 2016. 4

[17] Haifeng Yuan, Saumyakanti Khatua, Peter Zijlstra, Mustafa Yorulmaz, and Michel Orrit. Thousand-fold enhancement of single-molecule fluorescence near a single gold nanorod. *Angewandte Chemie International Edition*, 52(4):1217–1221, 2013. 2, 6

[18] Taishi Zhang, Nengyue Gao, Shuang Li, Matthew J Lang, and Qing-Hua Xu. Single-particle spectroscopic study on fluorescence enhancement by plasmon coupled gold nanorod dimers assembled on dna origami. *The journal of physical chemistry letters*, 6(11):2043–2049, 2015. 6

[19] P Zijlstra and M Orrit. Single metal nanoparticles: optical detection, spectroscopy and applications. *Reports on Progress in Physics*, 74(10):106401, 2011. 1, 5

Appendix A

More detailed setup

A.1 Slide preparation protocol

A 22 × 40 mm microscopy slide is thoroughly cleaned by first bathing it in a ultrasound bath immersed in methanol. Then the slide is flushed with ethanol and then with methanol. After flushing the slide is blown dry with nitrogen. The slides are activated by an oxygen plasma to create -OH groups on the surface. Then the slides are bathed is a (3-Mercaptopropyl)trimethoxysilane (MPTMS) diluted with ethanol to about 5%. The MPTMS binds with the -OH groups on the surface and the gold nanorods can bind to the -SH groups of the MPTMS.

10 μL of 650-CTAB AuNR solution is diluted by 20 with a 190μL 1 mM CTAB solution to prevent them from clustering. 20 μL of 100μM tris(2-carboxyethyl)phosphine (TCEP) is added. To prevent clustering of the nanorods. 30μL of the gold nanorod solution is added on each slide and spin-coated. Afterwards the slides are cleaned with PBS and demineralised water to get rid of the CTAB layer around the goldnanorods.

A docking (D) and antifouling (A) strand are diluted with a citric acid buffer to 5 μM. The imager (I) is diluted with buffer C to 500pM solution. The docking and antifouling solutions are mixed and a droplet of the mixture is placed on a slide with gold nanorods to incubate it.

A.2 Measurement protocol

The incubated slide is placed in a flow cell and demineralised water is flushed through the flow cell until it is filled. A prism with a drop of microscopy oil is placed on the top of the flow cell. a drop of demineralised water is placed on the lens. The slide is illuminated with white light. The resonance spectrum of the nanorods is first measured by saving an image of the microscope passing through different wavelength filters. These images are then processed by a Matlab script. For every individual particle a 2D Gaussian curve is fitted over the intensity of the particle. These intensities for different wavelengths are then combined to fit the spectrum of the particle.

To measure the fluorescence enhancement, an imager is passed through the flow cell. A video is captured of a section of the slide. And for every particle the intensity around the particle is analysed over time. It is expected that the measured intensity increases significantly when a fluorescent particle binds to the correct part of the nanorod. Also, the fluorescence of the phluorophores without the influence of nanorods is measured by simply taking a video of the same imager passing along a slide which is prepared identically to the nanorod slides except for the spincoating of the nanorods.